2025 SPE Oman Petroleum & Energy Show (OPES)

SPE-224998-MS

A Multi-Scale Evaluation of Polymer Injectivity and Fracture Behavior in the Burgan Field

Mohammad B. AlAbdullah[1], Meshal Algharaib[1], Randall S. Seright[2], Abbas Sanaseeri[3]

[1] Kuwait University, Kuwait
[3] New Mexico Institute of Mining & Technology, Socorro, NM, USA
[5] Kuwait Oil Company, Ahmadi, Kuwait

Abstract

This paper provides a comprehensive analysis of polymer injectivity in the Burgan field, the world's largest sandstone oil field, particularly the Wara reservoir. Polymer flooding in the Wara formation is a strategic objective for the field plan to reach the Kuwait oil production target. The study provides corefloods, rheological polymer measurements, fracture pressure field measurements, and long-term polymer field injectivity tests. All the data have been critically evaluated using analytical models to assess the polymer injectivity and potential fracture initiation and extension.

Laboratory measurements of polymer bulk and in-situ viscosity were conducted using viscometers, while corefloods assessed HPAM polymer viscoelasticity under reservoir conditions (55°C, 162,000 ppm TDS). Step-rate tests in the field determined fracture initiation pressures, and long-term injectivity tests were performed in three wells at multiple rates. Field pressure responses were analyzed alongside coreflood results using the Unified Viscoelastic Injectivity Model (UVIM) coupled with a PKN fracture model. Fluids flow-back analysis assessed polymer degradation, and geomechanical studies provided insights into fracture direction. This integrated approach ensured a thorough understanding of fracture initiation and polymer behavior.

Initial predictions suggested that no fractures would occur during polymer injection. However, detailed analyses revealed that fractures were indeed occurring. This conclusion was drawn by comparing polymer injectivity at various polymer concentrations with water injectivity. Polymer injectivity was found independent of polymer concentration—indicating potential in-situ fracture formation due to polymer viscoelasticity. Laboratory coreflood experiments confirmed these findings, demonstrating that when the injection velocity exceeds 40 ft/day, the polymer's extensional viscosity increases due to viscoelastic effects. As a result, the calculated pressure surpasses the fracture pressure of 2500 psi (as measured in step-rate tests). The UVIM fracture model estimated a fracture extension of approximately 80 ft from the well. These findings are crucial for the effective planning of field-scale polymer flooding. The analysis indicates a need to clearly define the objective and design of polymer flooding within a high permeability contrast reservoir.

This study provides critical insights into polymer injectivity and fracture management in the world's largest sandstone oil field. It offers a novel, data-driven workflow for optimizing polymer flooding, addressing fracture risks from lab to field scale. The findings are vital for enhancing polymer flooding efficiency and improving field-scale implementation, contributing significantly to the petroleum industry's understanding of polymer-induced fracture behavior.

Introduction

Polymer viscoelasticity and injectivity literature

Polymer flooding is considered one of the most successful chemical-enhanced oil recovery (EOR) methods, aiming to increase aqueous phase viscosity to improve oil sweep efficiency. Synthetic polymers (e.g., HPAM) are commonly used for field implementation due to their availability and low cost. Their non-Newtonian and viscoelastic rheological behavior makes predicting their in-situ injectivity a non-trivial problem in the field (Seright et al. 2009).

HPAM polymers exhibit shear-thinning behavior, where viscosity decreases as shear rates increase. Additionally, their viscoelastic properties in porous media play a pivotal role in determining flow characteristics. These properties become more pronounced with higher molecular weights and polymer concentrations (Qi et al. 2017; Erincik et al. 2018). Viscoelasticity is a time-dependent phenomenon involving the relaxation and contraction of polymer chains during flow. If the polymer relaxation time exceeds the residence time, the polymer chains remain entangled, resulting in shear-thickening and increased viscosity. Residence time is inversely proportional to shear rate or fluid velocity (Azad 2022).

This elongational rheological behavior is especially critical near the injection well, where fluid velocities are highest. Shear-thickening or elongational viscoelastic behavior occurs at high rates (Seright 1983; Delshad et al. 2008; Glasbergen et al. 2015; Seright et al. 2023), raising aqueous phase viscosity. Such behavior can significantly decrease injectivity as the aqueous phase viscosity increases (Wang et al. 2008; Seright et al. 2009). However, field studies often reported improved injectivity under such conditions. This improvement is attributed to the initiation of fractures around the wellbore, induced by elevated injection pressures that exceed the reservoir's parting pressure (Clemens et al. 2013; Manichand et al. 2013; Zechner et al. 2015; Melo et al. 2017; Seright 2017; Dandekar et al. 2021).

Sagyndikov et al. (2022) reviewed over 43 years of polymer flooding field trials, finding that elongational viscosity near the injector causes fractures in all vertical injection wells. The orientation and extent of these fractures are critical for polymer sweep efficiency. If fractures extend more than one-third of the inter-well distance and align toward the producer, the sweep efficiency can be significantly compromised (Dyes et al. 1958; Lee 2012; Seright 2017).

In this study, polymer injectivity and fracture propagation in the WARA formation of the Greater Burgan field are systematically examined. The analysis combines laboratory-scale studies of polymer bulk and in-situ rheology, analytical models based on the Darcy equation and viscoelastic injectivity model (Abdullah et al. 2023a; Abdullah et al. 2023b), and field injectivity tests integrated with geomechanical stress orientation assessments. These approaches aim to predict polymer-induced fracture initiation and growth while evaluating fracture extension and direction in the WARA formation.

Reservoir background

The Wara formation is part of the Greater Burgan field in Kuwait, the second-largest field in the world. The field’s oil production started in 1946 with high productivity due to the exceptional Darcy permeability of the Burgan and Wara formations. The field's daily production is approximately 70% of Kuwait's daily oil production. The Wara formation is a significant contributor to the field’s production (Al-Murayri et al. 2022). The Wara formation consists of multiple sandstone layers, with a gross thickness ranging from 140 ft to 180 ft and exhibiting vertical and horizontal variations in lithology. In 2014, water injection started maintaining reservoir pressure, which had declined below the bubble point pressure. Feasibility studies have demonstrated Wara’s significant potential for chemical EOR, specifically highlighting strategic field development efforts—such as assessing polymer flooding as an extension to water flooding (Al-Murayri et al. 2021). Three long injectivity tests were conducted with water and polymer injection in the Wara formation. The tests aimed to assess polymer injectivity and maximum allowable injection rate and pressure for further field implementation (Al-Murayri et al. 2022; Al-Qattan et al. 2024).

General Characteristics of the Wara Formation (Al-Murayri et al. 2021; Al-Qattan et al. 2024):

- Depth (ft): 4000 (datum)
- Porosity: 0.10–0.25
- Horizontal permeability (mD): 0.004–5000 mD
- Initial pressure (psi): 2100 (@datum)
- Current pressure (psi): 1600 (@datum)
- Temperature (°C): 55 (@datum)
- Connate water salinity (ppm TDS): 160,000
- Wettability: Water wet
- Oil viscosity at reservoir temperature (cp): 3
- Stock Tank Oil API Gravity: 27–30

Methodology

Experimental work

To evaluate polymer injectivity, we investigated the rheological properties of polymer solutions in a viscometer and in-situ porous media. We utilized the same polymer and conditions for the injectivity tests. ZLPAM-40520 polymer was used with a molecular weight ranging from 5 to 10 million Daltons and contains 15–20% ATBS/AMPS (Al-Murayri et al. 2022). The brine used in the experiments was a synthetic composition based on field-available brine, as detailed in Table 1. A polymer solution with a concentration of 1800 ppm was prepared, and its viscosity (versus shear rate) was measured at temperatures of 25 °C and 55 °C using Brookfield LVDV-II+Pro viscometer (**Figure 1**). Single-phase coreflood experiments were conducted by sequentially injecting water and polymer solution. The maximum fluid velocity tested was 200 ft/day, approximating the calculated Darcy velocity at the perforation on the zone of interest of well-A. Water injection commenced at the lowest Darcy velocity of 1 ft/day and was gradually increased to the maximum velocity of 200 ft/day to determine permeability and assess inertia effect occurrence at the highest rates. Subsequently, polymer injection was initiated at the highest rates, and then gradually decreased to the lowest rates. Although the reservoir temperature is 55 °C, temperature logs indicated a cooling effect from historical water injection to approximately 30 °C. Therefore, since the primary focus of this paper is to examine fracture extension caused by polymer viscoelasticity, we considered the room temperature to be an approximation of the near-wellbore temperature. **Figure 2** illustrates the experimental set-up; three fluid accumulators are connected to achieve the high injection velocities required.

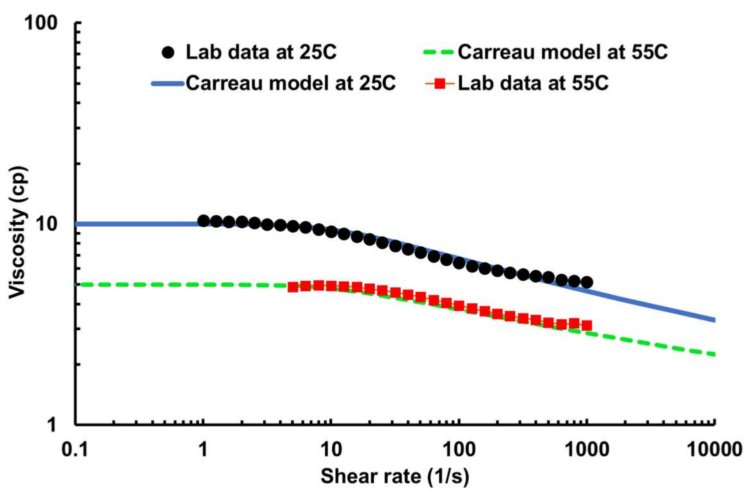

Figure 1—ZL-40520 bulk viscosity measured at 25 °C and 55 °C.

Table 1—Synthetic brine composition.

Composition	Concentration (ppm)
NaCl	124,211.36
$CaCl_2$	25,823.87
$MgCl_2$	8868
KCl	3386.08
$SrCl_2$	591.64
Total salinity	162,880.95

Table 2—Core properties and conditions.

Core Type	Bentheimer (SS-102)
Length, cm	15.15
Diameter, cm	3.773
A, cm^2	11.181
Dry Weight, gm	339.34
Pore Volume, cc	41
Porosity, %	24
Temperature, °C	Room
Confining pressure,	1500
Polymer	ZLPAM-40520

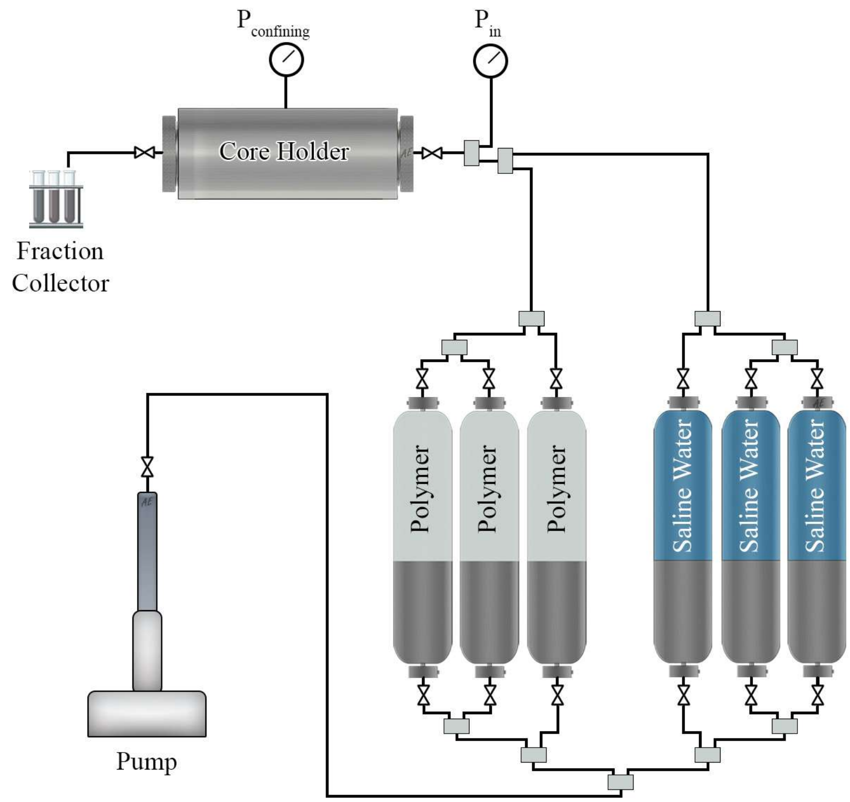

Figure 2—Coreflood experimental set-up.

Well-A

In this study, we focus our analysis on Well-A in the Wara formation within the Greater Burgan Field. Well-A was perforated at four distinct layers, each exhibiting permeability values that vary more than an order of magnitude (24–659 mD) (**Figure 3**). Step-rate polymer injection tests were conducted in Well-A and are thoroughly documented in Al-Murayri et al. (2022). As shown in **Table 3,** acid stimulation was performed before polymer injection to reduce wellbore skin. Injection Logging Tool (ILT) measurements were taken at various stages throughout the injectivity tests to assess effective reservoir thickness, fluid distribution across the perforated layers, and conformance improvements during polymer injection. Four ILTs were conducted. The first three were during the waterflood, and the last one (December 2021) was with 1500 ppm polymer injection at 2500 bpd. The ILT results showed over 86% of fluid intake is through the bottom layer (Table 4). After polymer injection, a slight enhancement in conformance was observed within the bottom layer from the December ILT when compared with the prior ILT during water injection in November 2021 (**Figure 3**)

Additionally, three fall-off tests (PFO) were conducted before polymer injection to evaluate formation permeability and the skin factor. Polymer injectivity was assessed using polymer concentrations ranging from 600 to 2000 ppm and injection rates between 2000 to 3600 barrels per day (bpd) (Table 3).

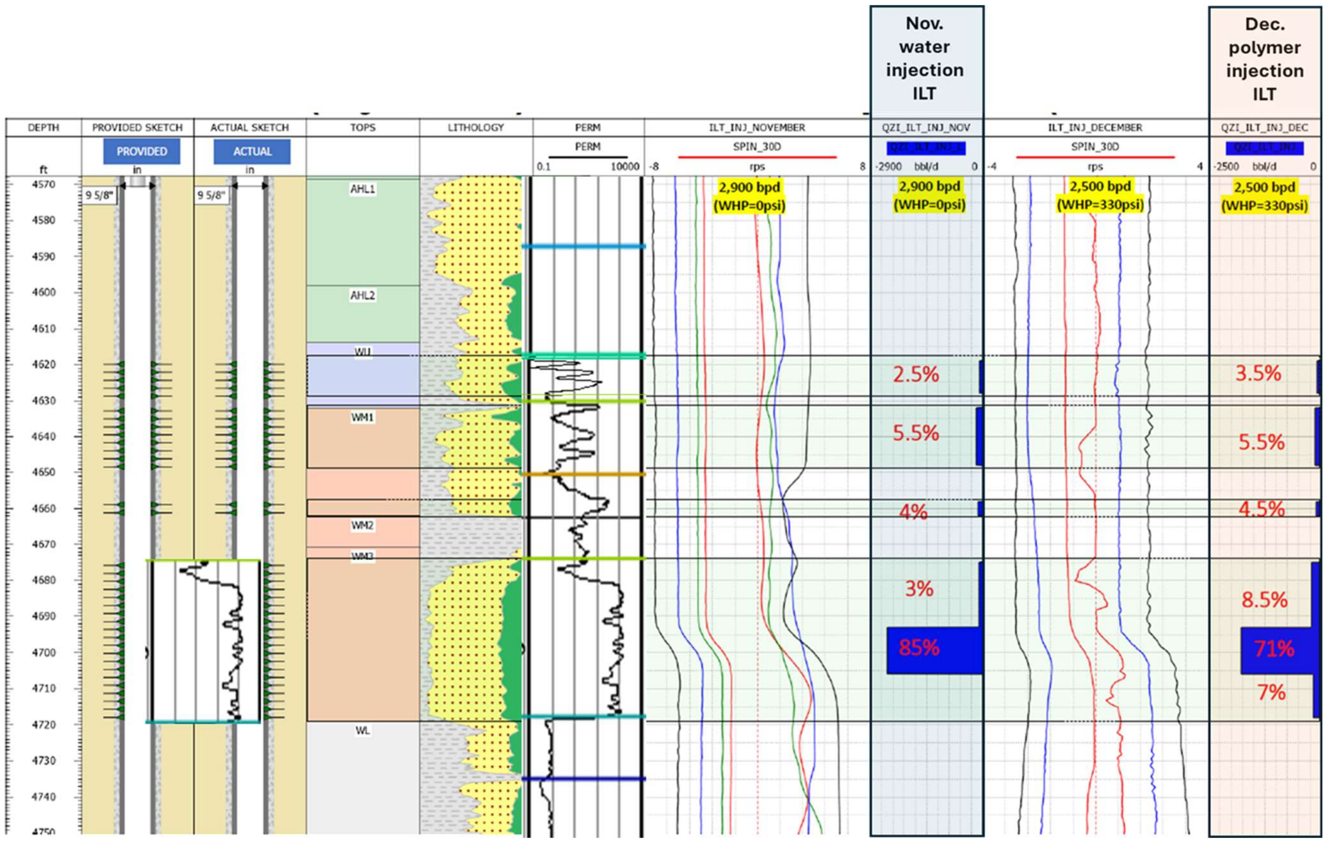

Figure 3—Well-A well-log showing from left to right tracks: ILT, perforation zones, lithology, and permeability for 2021 ILT. November ILT in the blue box shows 88% in the lower zone within two subzones, and December shows a total of 86.5% but is more segmented into three subzones.

Table 3— Schedule of events in well-A.

Stage	Date	Polymer concentration (ppm)	WHP (psi)	BHP (psi)	Injection rate (bbl/day)
ILT	18/08/2021	-	-	-	-
PFO	27/08/2021	-	-	-	-
ILT	06/09/2021	-	-	-	-
Acid Stimulation	13/10/2021	-	-	-	-
Post-acid PFO	14/10/2021	-	-	-	-
Begin water injection	18/11/2021	-	-	-	-
PFO	26/11/2021	-	-	-	-
ILT	27/11/2021	-	-	-	2900

First polymer injection	3-10/12/2021	600	210-430	2124-2159	4000-2000-2500 -3000-4500-2000
Second polymer injection	10-17/12/2021	900	314-420	2457-2579	4000-6000-2000
Third polymer injection	17-23/12/2021	1200	314-464	2457-2537	2000-4000-6000
Fourth polymer injection	23/12/2021-14/02/2022	1500	228-364	2352-2500	2000-4000-3000-3750 -3000-3400-3200-3500-3400-3300-3400-3200-3400-3500-3600
ILT	12/29/2021	1500			2500
Fifth polymer injection	14-22/02/2022	1800	308-365	2450-2500	2600-2800-3000-3200
Final polymer injection	22-25/02/2022	2000	320-362	2460-2495	2500-2800-3000-3100

Table 4— Well-log average permeability and ILT fluid intake results from December 2021 during 1500ppm polymer injection.

Permeability (mD)	**Top (ft)**	**Bottom (ft)**	**Zone**	**Perforated thickness (ft)**	**ILT (%)**
47	4619	4628	(1) WU	9	3.5
24	4632	4648	(2) WM1	16	5.5
186	4658	4662	(3) WM2	4	4.5
659	4675	4718	(4) WM3	43	86.5

Injectivity Analysis Interpretation

This study aims to analyze field injectivity measurements by integrating data from recently conducted laboratory experiments with analytical/semi-analytical models. Specifically, the results from core flood experiments will be utilized to characterize the viscoelastic properties of the polymer. These characterizations will enable us to predict the polymer's in-situ behavior using our analytical/semi-analytical models described below.

1. Determine fracture initiation based on Darcy radial flow

The first approach involves calculating reservoir injectivity using Darcy's radial flow model and comparing these calculations with injectivity measurements obtained from the field. This comparison serves as a criterion to determine whether the fluid flow adheres to a radial flow pattern or transitions to a linear flow pattern due to fracture propagation. By analyzing the alignment or discrepancies between the modeled and measured injectivity, we can identify the dominant flow regime within the reservoir. The criterion is defined as such:

$$\left[\frac{q}{\Delta p}\right]_{measured} >> \left[\frac{\sum kh}{141.2\mu \ln\left(r_e/r_w\right)}\right]_{calculated} \tag{1}$$

In this equation, q represents the injection or production rate (bpd), Δp is the pressure drawdown (psi), k denotes permeability (md), h is the formation height (ft), μ represents fluid viscosity (cp), r_e is the external drainage radius (ft) or approximated as half the distance to nearest well, and r_w is the wellbore radius (ft). It is worth noting this model follows Darcy equations assumptions; besides, it assumes that the fluid viscosity is filling the whole drainage radius. We account for near-wellbore skin (s) using an equivalent wellbore radius $r_{we} = r_w e^{-s}$.

2. Determine fracture initiation and length with UVIM-PKN model

Abdullah et al. (2023a) presented a semi-analytical model to calculate injectivity called the unified injectivity model (UVIM) that accounts for polymer elongational viscosity in the Darcy equation using the unified viscoelastic polymer rheology model (Delshad et al. 2008), describes as below:

$$\mu_{\text{app}} = \mu_\infty + \left(\mu_p^0 - \mu_w\right)\left[1 + (\lambda\dot{\gamma}_{\text{eff}})^2\right]^{\frac{n-1}{2}} + \mu_{\text{max}}\left[1 - \exp\left(-\left(\lambda_2 \tau \dot{\gamma}_{\text{eff}}\right)^{n_2 - 1}\right)\right], \tag{2}$$

where μ_∞ (cp) is the polymer viscosity at high shear rates that is assumed equivalent to water viscosity, μ_p^0 (cp) is the polymer viscosity at low shear rates, μ_w (cp) is the water viscosity, μ_{max} (cp) is the maximum polymer viscosity in shear-thickening, n_2 is the exponent associated with the shear-thickening behavior, λ shear-thinning parameter (sec $^{-1}$), λ_2 shear-thickening parameter = 0.01 (unitless) (Zeynalli et al. 2022), and τ approximates insitu viscoelastic relaxation time (sec). The effective shear rate $\dot{\gamma}_{eff}$ (sec $^{-1}$) in the reservoir is given by (Cannella et al. 1988):

$$\dot{\gamma}_{\text{eff}} = \left[\frac{3n+1}{4n}\right]^{\frac{n}{n-1}} \left[\frac{4CU_r}{\sqrt{8kk_{rw}S_w\phi}}\right], \tag{3}$$

where n is the shear-thinning exponent. C is a correction factor that converts bulk polymer viscosity measured in the viscometer into insitu polymer rheology.

The UVIM model is coupled with 2-D fracture models: Perkins-Kern-Nordgren (PKN) to predict fracture length for viscoelastic polymers. This model calculates polymer viscosity. The model assumes that water is injected into the reservoir until reaching a steady-state and residual oil saturation, which is a reasonable assumption as most of polymer thickening behavior is around the wellbore where oil is well-swept. Then the polymer is injected (**Figure 4**). Throughout polymer injection, the BHP of the injection well increases while the outer boundary pressure (P_e) remains constant. Total pressure drop (ΔP_T) is the summation of the polymer pressure drop between the wellbore and the extent of the polymer slug (ΔP_p), calculated from UVIM, and water pressure drop (ΔP_w) from the polymer slug face to the reservoir boundary, calculated from Darcy's law.

$$\Delta P_T = \Delta P_p + \Delta P_w = BHP - P_e. \tag{4}$$

ΔP_p is calculated up to the polymer propagation radius (r_p) by solving the UVIM integral discussed in detail in Abdullah et al. (2023a), ΔP_w is calculated from r_p to r_e using Eq. (1).

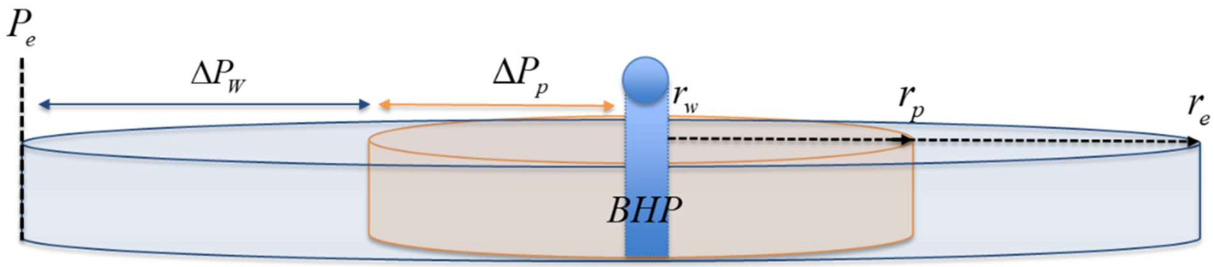

Figure 4—Schematic diagram of the UVIM conceptual reservoir model. The diagram illustrates the assumption that the reservoir is waterflooded (blue region) until reaching a steady-state and to the residual oil saturation, then the polymer is injected (orange region) (Abdullah et al. 2023a).

The fracture propagation criteria when coupling the UVIM with PKN shall satisfy the following conditions:

$$BHP > \frac{K_{IC}}{\sqrt{\pi A_f}} + p_f. \tag{5}$$

Where bottom-hole pressure (BHP) is calculated from Eq. (4) from the UVIM, p_f is the fracture pressure in psi, K_{IC} is the fracture toughness that is related to fracture surface energy (typically 500 - 2000 psi.inch0.5(Gidley and Engineers 1989, Economides and Nolte 2000)), A_f is the fracture geometry parameter (if $2L_f > h_f$ then $A_f = h_f / 4$, or if $2L_f < h_f$ then $A_f = L_f$). The fracture pressure and geometry are calculated using the PKN model, as discussed in Abdullah et al. (2023a).

The UVIM-PKN model assumes a constant pressure condition at the reservoir boundary, with the BHP dynamically updated in UVIM using an equivalent wellbore radius as proposed by Prats (1961). The simplified fracture model is based on the following assumptions: the reservoir is homogeneous, single-layered, and exhibits single-phase flow, with oil at residual saturation. Flow follows a radial or pseudo-radial pattern in a vertical well. The fracture is vertical, bi-winged, and maintains a constant height equivalent to the reservoir thickness. Fluid leak-off from the fracture faces occurs uniformly, and a power-law model models the polymer rheology within the fracture.

Results and discussion

Lab results

The ZL-40520 polymer showed a viscoelastic behavior when injected at multiple velocities, with a maximum elongational viscosity of 65 cp (**Figure 5** and Table 5). The coreflood results showed shear thickening behavior when injecting above 6 ft/day (Figure 6), corresponding to 30ft of polymer slug radius. Thus, from the wellbore to a 30 ft radius, shear thickening is expected to dominate the polymer insitu rheology assuming injecting at 3200 bpd (Figure 7).

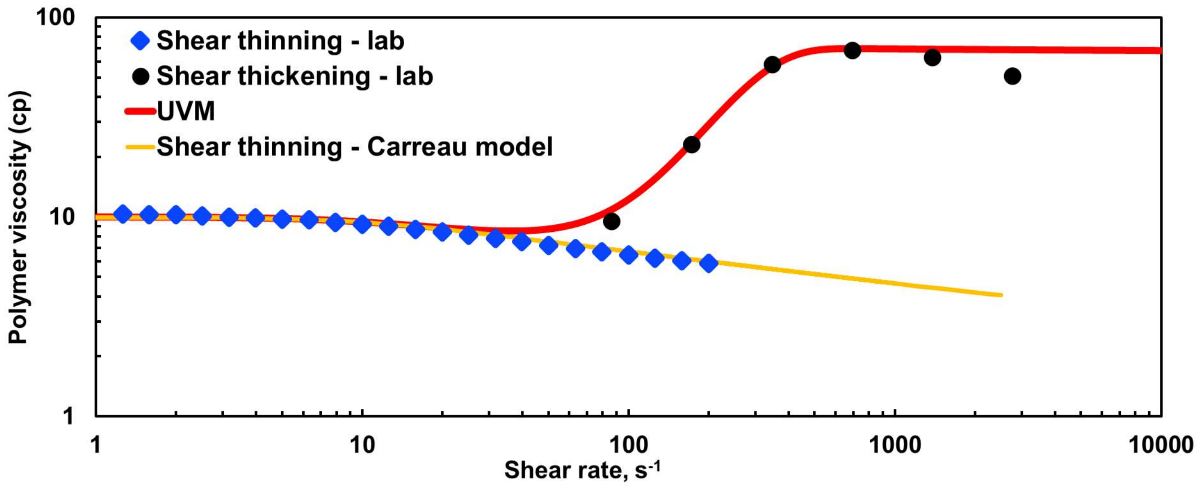

Figure 5—Lab coreflood results for ZLPAM-40520 polymer showing viscoelastic behavior (blue triangles for shear thinning and black dots are shear-thickening), while the Carreau model fit in the yellow curve and UVM fit in the red curve.

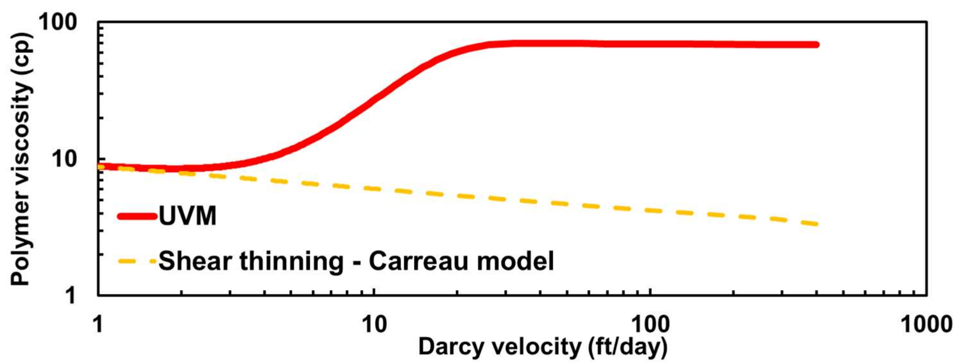

Figure 6—Calculated in-situ polymer viscosity vs. Darcy velocity for ZLPAM-40520 polymer at 3200 bpd based on UVM in solid red curve, while the Carreau shear thinning model is in the yellow curve.

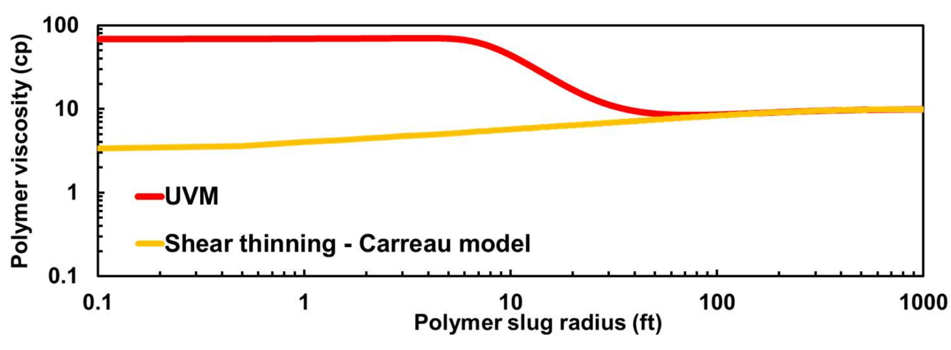

Figure 7—Calculated in-situ polymer viscosity vs. polymer slug radius for ZLPAM-40520 polymer at 3200 bpd based on UVM in solid red line, while the Carreau shear thinning model is in the yellow curve.

Table 5—UVM parameters used to match lab-measured polymer viscosity.

Shear thinning parameters			Shear thickening parameters		
μ^{∞}	1.1	Infinite shear rate Viscosity (cp)	n_2	3.3	Shear thickening parameter
n	0.8	Shear thinning Index	μ_{max}	65	Max shear thickening viscosity (cp)
μ_p^0	10	Zero shear rate viscosity [cP]	λ_2	0.01	Shear thickening parameter
λ	0.1	Shear thinning parameter (cp)	τ	0.35	Polymer relaxation time (sec)

Re-evaluating field injectivity data

When evaluating the injectivity test results from Al-Murayri et al. (2022), we considered the water injectivity at 4188 bpd with bottom-hole pressure (BHP) of 1914 psi as a reference water injectivity (in the y-axis denominator of **Figure 8**). In **Figure 8**, by plotting the actual field injectivity divided by the reference water injectivity at different injection rates, we noticed that for different polymer concentrations, the injectivity trends overlap. One would expect for matrix injection, as polymer concentration increases, the injectivity curves could have the same slope but with a greater y-axis intersection point. This clearly indicates that the change in injectivity is independent of polymer rheology and is positively correlated to the injection rate alone. Also, this scenario is expected when the injection area increases, similar to a fracture propagation behavior. Such observations led to further investigation using the earlier-mentioned analytical and semi-analytical tools.

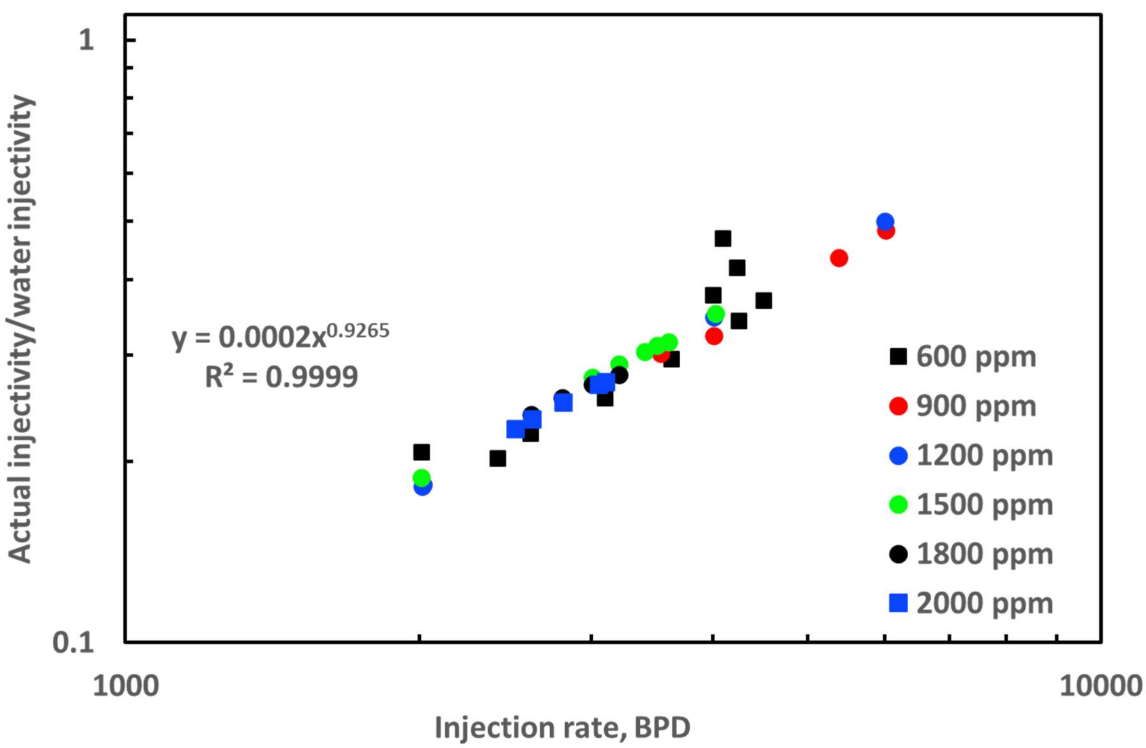

Figure 8—Actual injectivity divided by the reference water injectivity plotted vs injection rate at different polymer concentrations.

Fracture initiation based on Darcy radial flow

Linear (fracture-like) flow is likely when measured injectivity significantly exceeds the Darcy radial flow injectivity in Eq.(1). In our injectivity calculations, we focused on the near-wellbore rheology. Thus, we assumed three fluid viscosities by using viscosity values at room temperature corresponding to the observation of a temperature reduction from 55 °C to 30 °C due to historical water injection (Al-Murayri et al. 2022). The three viscosities used in the injectivity calculation are: (1) water viscosity was assumed to be 1.1 cp (black line in **Figure 9**), (2) polymer viscosity at 1800 ppm of 10 cp at 7.3 s^{-1} (assumed deep in the reservoir) and (3) 65 cp as maximum polymer viscosity due to elongational behavior near the wellbore (>300 s^{-1} or >25 ft/day) at 1800 ppm. Since the Darcy radial equation here assumes a single viscosity over the drainage radius, we will vary the drainage radius between 10 to 400 ft in **Figure 9** (a) to (d). A skin factor of 5 is used to match the calculated injectivity with the measured water injectivity at a reference point of 4188 bpd (black square overlays the black solid line in Figure 9). This skin factor value agrees with fall-off tests interpreted values (from internal reports). As described in Eq.(1), linear flow is expected whenever the measured injectivity exceeds the calculated injectivity for radial flow.

In Figure 9 **(a),** based on a 400 ft drainage radius, shows that if there is no shear thickening near the wellbore, the measured polymer viscosity at a shear rate of 7.3 s^{-1} (blue line) indicates linear flow for all polymer concentrations once injection rates exceed ~2000 bpd. Conversely, linear flow is expected across all concentrations with shear thickening near the wellbore (orange line). Figure 9 (b) shows that at a drainage radius of 100 ft, injecting above 2000 bpd similarly results in linear flow for 10 cp polymer viscosity. Figure 9 (c) assumes a conservative scenario where the polymer reaches only 50 ft at an injection rate of 3200 bpd within the 43 ft effective target thickness. It demonstrated that injecting at rates above 2000 bpd leads to fracturing when polymer viscosity is 10 cp without considering shear thickening effects. Lastly, Figure 9 (d) focuses on the near wellbore region of 10 ft, typically dominated by shear thickening with Darcy velocities ranging from 40 to 200 ft/day. Injecting above ~1300 bpd in this region is likely to fracture the well, as it exceeds the threshold indicated by the dotted orange line. This comprehensive analysis underscores the critical injection rates and viscosity conditions necessary to maintain radial flow below the parting pressure.

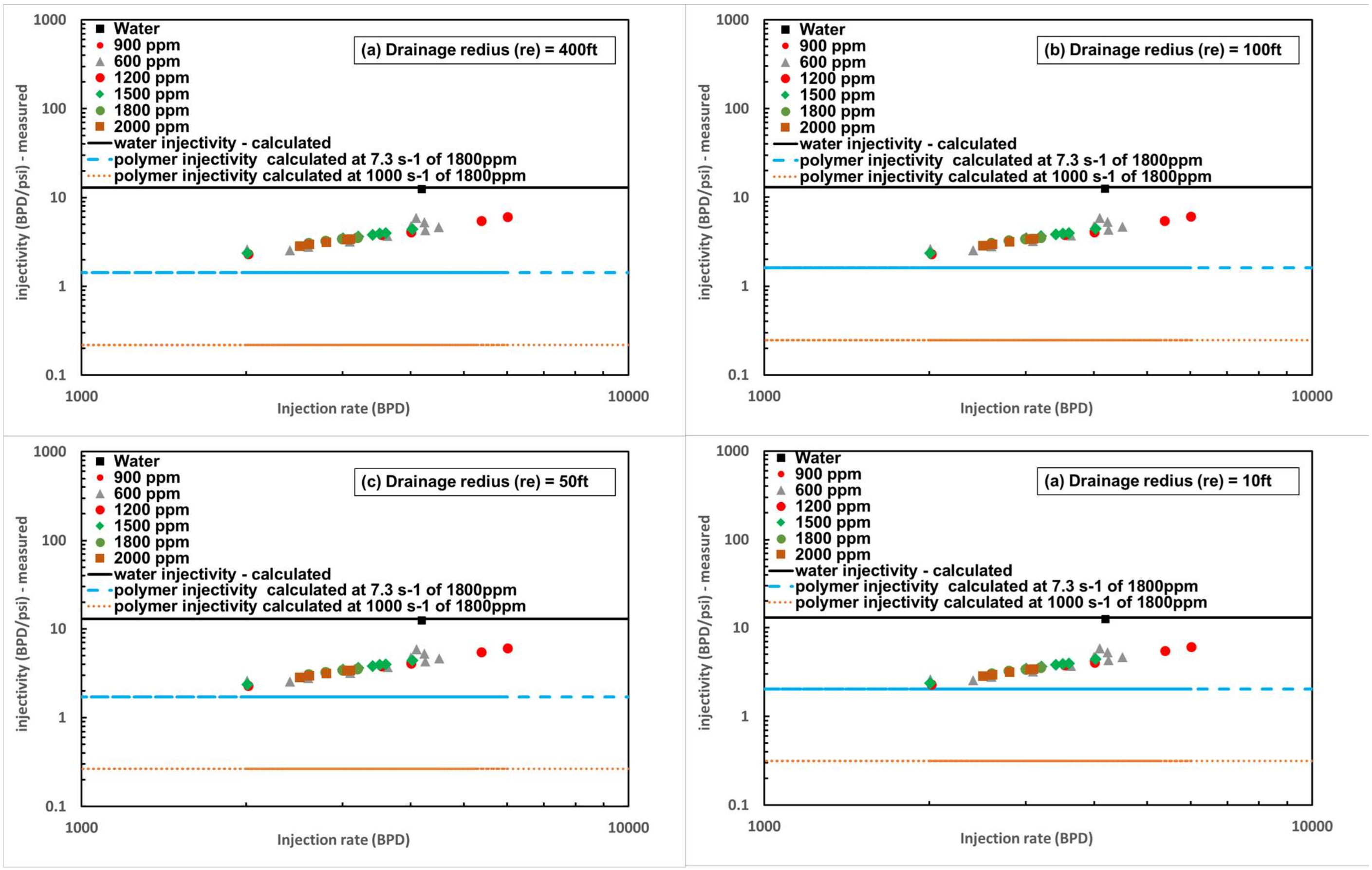

Figure 9— Comparing polymer measured injectivity from the long-term injectivity tests (in dots) at different concentrations and rates to calculated polymer injectivity (in lines) using Darcy radial equation at various drainage radii of 400ft, 100ft, 50ft, and 10ft from (a) to (d) respectively.

Determine fracture initiation and length with the UVIM-PKN model

Fracture initiation with UVIM-PKN model

To further confirm our observations, we considered the injected polymer concentration at 1800 ppm at 2600 - 3200 bpd (same conditions in the step rate test by (Al-Murayri et al. 2022)) and plotted polymer injectivity measured and calculated vs. injection rate (**Figure 10**). We calculated injectivity using the UVIM model in three scenarios at ~50 ft polymer slug radius: (a) shear thinning following Carreau (1972) model without fracturing (black triangles); (b) a viscoelastic polymer (shear thinning and thickening) following UVIM but without fracturing (back diamonds) ; (c) and lastly, a viscoelastic polymer with fracture propagation using the UVIM-PKN semi-analytical model (red-x's). As discussed earlier, UVIM calculates injectivity more accurately than Darcy radial flow equation, as it accounts for the change in viscosity with in-situ change of shear rate in the reservoir.

As expected, if no fracture is assumed, the calculated viscoelastic polymer rheology (black diamonds) is lower than the actual measured injectivity (green circles). The calculated UVM viscosity is lower due to the significant increase in elongational viscosity. The shear thinning injectivity (black triangles) exhibits a closer match to the measured injectivity, as the polymer follows a shear thinning rheology in fractures (Zechner et al. 2013). The minimal variation in injectivity (in both Carreau and UVM models) with injection rate is due to the small variation in the injection rate (between 2606 – 3200 bpd) that does not vary polymer viscosity significantly (green and orange lines in **Figure 11 (a) and (b)**). The calculated UVIM-PKN injectivity (red x's in Figure 10) matches the actual recorded injectivity. Although the polymer rheology follows a shear thinning behavior during fracturing, the UVIM-PKN calculated injectivity shows a higher increase in injectivity as the injection rate increases, compared to the Carreau plateauing behavior. This observation indicates an increase in the injection area due to fracture propagation and the change in polymer rheology. Table 6 lists the input parameters for the injectivity calculation.

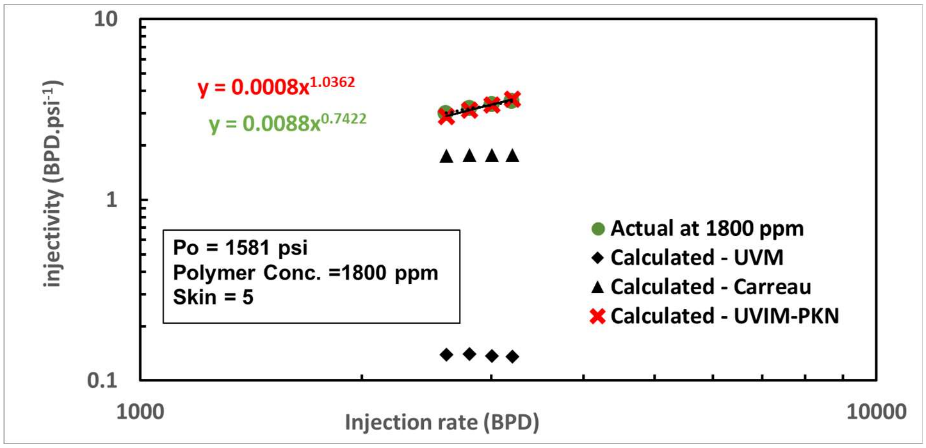

Figure 10— Measured (green circles) and calculated (black triangles for shear thinning without fracture and black diamonds for viscoelastic polymer without fractures, and red axes for viscoelastic polymer with fracturing) injectivity vs. injection rate at 1800 ppm polymer concentration.

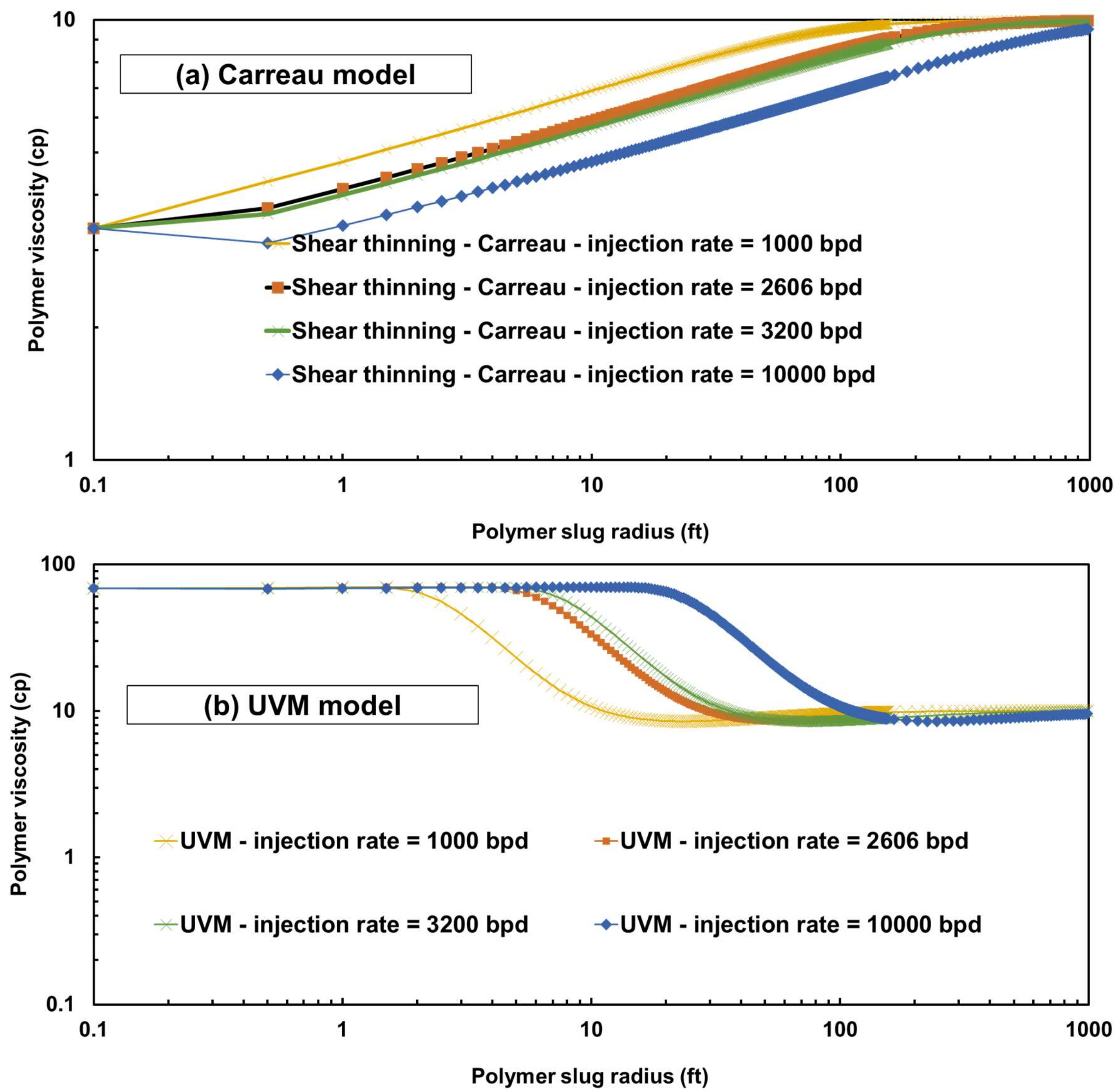

Figure 11—(a) Shear-thinning Carreau model polymer viscosity vs. polymer propagation radius. (b) Shear thinning and thickening UVM model polymer viscosity vs. polymer propagation radius.

Table 6—Parameters used in injectivity and fracture model UVIM-PKN

Parameter	Value	Parameter	Value
Injection rate (q), bbl/day	3200	Water Viscosity (μ_w), cp	1.1
Permeability (k), mD	650	Polymer concentration (C_p), wt%	0.18
Formation thickness (h), ft	43	Fracture initiation pressure (p_{fi})	2500
Wellbore radius (r_w), ft	0.3	Minimum horizontal stress (psi)	2300
Skin factor	5	Power law exponent, n_p	0.8
Drainage radius (r_e), ft	400	Power law paramter (K), cp.sec$^{(n-1)}$	16
Boundary Pressure (P_e), psi	1581	Young's Modulus ('E), psi	1500000
Porosity (ϕ),%	0.18	Poisson's ratio (v)	0.21
Water saturation (S_w), %	0.7	Fracture thickness (h_f), ft	43
Water endpoint relative permeability (k_{rwo})	0.4	Turbulence parameter (C_{turb})	1.7
Correction factor (*C*)	1	Critical stress intensity factor (K_{IC}), ,psi.inch$^{0.5}$	2500

Fracture length with UVIM-PKN model

Since almost all the polymer injection field trials reviewed in the past 43 years indicate fracture initiation in vertical wells, the critical question becomes what the fracture extension and orientation are (Sagyndikov et al. 2022). If fractures extend over one-third of the inter-well distance and align toward the producer, the sweep efficiency can be significantly compromised (**Figure 12 (a)**). However, if the orientation is perpendicular to the injector-producer, we may expect enhancement in injectivity with slower front movement and better sweep efficiency (Figure 12 (b)) (Dyes et al. 1958; Gadde and Sharma 2001; Lee 2012; Seright 2017).

We history-matched the field bottomhole pressure (BHP) at 3,200 bpd and 1800 ppm between 14 and 22 February 2022. Using the UVIM-PKN model, we calculated a KH value of 24,580 md-ft based on the ILT effective thickness and log-measured permeability (Table 4). We considered a drainage radius of 400 ft fully saturated with water, while the polymer front extended to a radius of about 105 ft after 7 days. Prior field injections of lower-concentration polymer were excluded from our calculations. Under these assumptions, the model indicated a fracture half-length of approximately 90 ft—equivalent to one-tenth of the distance between well-A and its nearest offset well (**Figure 13**). Considering the ILT's effective thickness of 43 ft and elongational viscosity of 65 cp, the injection rate is relatively high, even at a permeability of 650 mD. Uncertain parameters such as minimum horizontal stress, Young's modulus, and critical stress intensity factor were tuned to match the recorded field BHP. A lab report received from the operator indicated a permeability reduction factor (RK) of 2.5 that would result in a fracture length of > 600 ft. This permeability reduction is highly unlikely for such a high-permeability rock (Vela et al. 1976; Seright 2017). Thus, we considered an RK of 1 in our calculations. Although fall-off tests were conducted at well-A, their early-time data were of poor quality, and it was hard to interpret fracture occurrence and length. Also, they were conducted only during the waterflooding period.

Considering that the nearest well is roughly 800 ft away from well-A and the maximum stress is oriented along the NW–SE direction, field operators can examine whether fracture extension will enhance, impair, or have minimal impact on large-scale polymer injection. High-quality fall-off tests conducted after the planned polymer injection could verify the extent of fracture propagation. In addition, combining these well tests with further geomechanical measurements—such as minimum horizontal stress magnitude and other rock properties—will help to monitor fracture growth accurately.

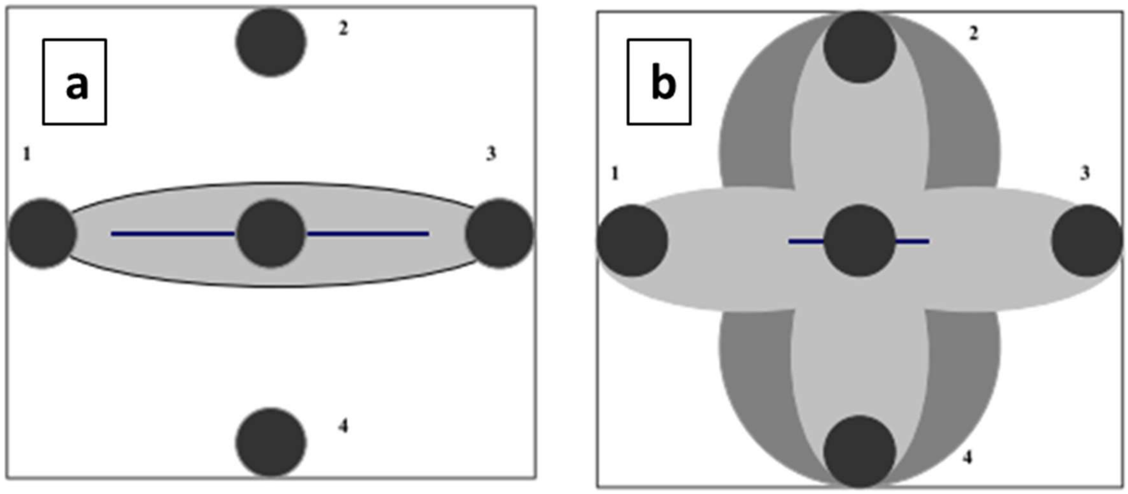

Figure 12—5-spot pattern with central injector and 4 producers showing fracture extension in the red line. (a) Weaker sweep efficiency with long fractures oriented to producers 1 and 3. (b) Improvement in sweep for producers 2 and 4 compared to (1) and (3). Adopted from Gadde and Sharma (2001).

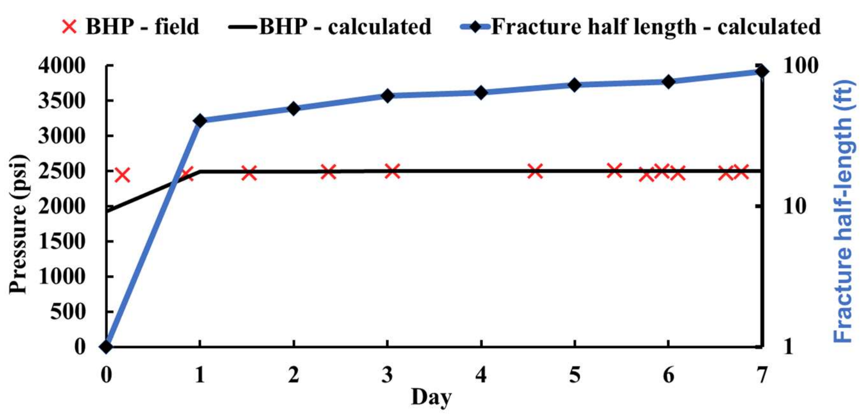

Figure 13— History matching the field BHP (red x's) with UVIM-PKN model (black solid line), resulting in fracture half-length of ~80ft (blue solid lines on right y-axis).

Re-evaluate The Purpose of Polymer Injection

The goal of switching from water flooding to polymer flooding should be well-defined. The lower formation in Wara (Figure 3) showed that even after polymer flooding ~90% of injection intake was into the bottom high permeability layer. When calculating the end points mobility ratio, it is 0.25, assuming oil viscosity of 3 cp, polymer viscosity of 4.7-10 cp (targeted polymer viscosity for full-field (Al-Qattan et al. 2024)), with the water and oil endpoints of 0.4 and 1 respectively. These values result in a favorable ratio (i.e., below unity), but considering the high permeability ratio between the bottom layers and the other layers (ranging from 4 to 27 between the various layers, Table 4), a mobility ratio decreased up to 0.03 (polymer viscosity of 40 cp) could further improve the conformance across the layers (Seright 2017). Injection of a polymer this viscous might be operationally challenging due to injectivity restriction and the potential for excessive fracture extension. In such a case, other conformance control strategies should be considered.

Summary and Conclusions

Analytical models, including Darcy radial flow and the viscoelastic injectivity model (UVIM), were employed to evaluate the onset of non-radial flow and fracture initiation. The results indicate that fracture-like flow is observed at polymer concentrations of 1800 ppm and injection rates exceeding 2000 bpd. Additionally, the UVIM-PKN model, validated against field data, predicts fracture propagation trends, showing that fracture half-lengths can extend up to 90 ft, approximately one-tenth of the distance to the nearest offset well. The findings of this study can be listed as follow:

1. If no fractures or fracture-like features were present, HPAM polymer flooding in the WARA formation would exhibit significant viscoelastic effects, which would dramatically influence injectivity. Thus, formation of fractures or fracture-like features during polymer injection is likely.
2. Laboratory and analytical modeling indicate that non-radial (fracture-like) flow dominates at high polymer concentrations and injection rates exceeding 2000 bpd.
3. The UVIM-PKN model effectively predicts fracture propagation that extends ~80 ft by matching field injectivity data.
4. Fracture orientation plays a crucial role in polymer sweep efficiency, with perpendicular fractures benefiting injectivity while minimizing negative impact on displacement efficiency.
5. Further assessment of the purpose of polymer flooding is needed for the Wara formation, as insignificant conformance enhancement is observed, with permeability contrast reaching 27 times between the layers.
6. Conformance control with polymer flooding might require injecting up to 40-cp polymer to overcome the permeability contrast, which could be infeasible.
7. High-quality fall-off tests and further geomechanically assessments are necessary to monitor fracture growth accurately and optimize large-scale polymer injection strategies, especially after polymer injection.
8. This study provides valuable insights into the complex interplay between polymer rheology, injectivity, and fracture propagation, assisting field operators in optimizing polymer flooding performance in the Greater Burgan field.

Acknowledgment

The authors would like to acknowledge Kuwait Oil Company's (KOC) management for granting permission to publish this work and the Enhanced Oil Recovery Center at Kuwait University (KUEORC) for facilitating the lab experiments.

References

Abdullah, M.B., Baqer, S., Delshad, M. *et al.* 2023a. Unified Viscoelastic Injectivity Model: Analytical Solutions Predicting Polymer Excess Pressure and Fracture Initiation. *Geoenergy Science and Engineering*, **221**, 111259, https://doi.org/https://doi.org/10.1016/j.petrol.2022.111259.

Abdullah, M.B., Seright, R.S., Machado, M.V.B. *et al.* 2023b. An Analytical Tool to Predict Fracture Extension and Elastic Desaturation for Polymer Field Projects. *SPE Annual Technical Conference and Exhibition*.

Al-Murayri, M.T., Kamal, D.S., Al-Qattan, A. *et al.* 2021. A practical and economically feasible surfactant EOR strategy: Impact of injection water ions on surfactant utilization. *Journal of Petroleum Science and Engineering*, **201**, 108479, https://doi.org/https://doi.org/10.1016/j.petrol.2021.108479.

Al-Murayri, M.T., Al-Qattan, A., Hassan, A.A. *et al.* 2022. First Polymer Injectivity Test in the Wara Formation of the Great Burgan Field: Strategic Milestone to Fast-Track Phased Commercial Polymer-Flooding Development. presented at the ADIPEC.

Al-Qattan, A., Al-Murayri, M., Almahmid, N. *et al.* 2024. First Long-Term Polymer Injectivity (LTPI) Test in Magwa Field Targeting Medium Quality Formation in Wara, Great Burgan Field. *International Petroleum Technology Conference*.

Azad, M.S. 2022. Characterization of Nonlinear Viscoelastic Properties of Enhanced Oil Recovery Polymer Systems Using Steady-Shear Rheometry. *SPE Journal*, 1-19, https://doi.org/10.2118/212824-PA.

Cannella, W.J., Huh, C. and Seright, R.S. 1988. Prediction of Xanthan Rheology in Porous Media. *SPE Annual Technical Conference and Exhibition*.

Carreau, P.J. 1972. Rheological Equations from Molecular Network Theories. *Transactions of the Society of Rheology*, **16**, 99-127, https://doi.org/10.1122/1.549276.

Clemens, T., Deckers, M., Kornberger, M. *et al.* 2013. Polymer Solution Injection - Near Wellbore Dynamics and Displacement Efficiency, Pilot Test Results, Matzen Field, Austria. presented at the EAGE Annual Conference & Exhibition incorporating SPE Europec, 2013/6/10/, London, UK.

Dandekar, A., Bai, B., Barnes, J. *et al.* 2021. Heavy Oil Polymer EOR in the Challenging Alaskan Arctic - It Works! , presented at the SPE/AAPG/SEG Unconventional Resources Technology Conference.

Delshad, M., Kim, D.H., Magbagbeola, O.A. *et al.* 2008. Mechanistic Interpretation and Utilization of Viscoelastic Behavior of Polymer Solutions for Improved Polymer-Flood Efficiency. presented at the SPE Symposium on Improved Oil Recovery, 2008/1/1/, Tulsa, Oklahoma, USA.

Dyes, A.B., Kemp, C.E. and Caudle, B.H. 1958. Effect of Fractures on Sweep-out Pattern. *Transactions of the AIME*, **213**, 245-249, https://doi.org/10.2118/1071-G.

Erincik, M.Z., Qi, P., Balhoff, M.T. *et al.* 2018. New Method To Reduce Residual Oil Saturation by Polymer Flooding. *SPE Journal*, **23**, 1944-1956, https://doi.org/10.2118/187230-PA.

Gadde, P.B. and Sharma, M.M. 2001. Growing Injection Well Fractures and Their Impact on Waterflood Performance. presented at the SPE Annual Technical Conference and Exhibition.

Glasbergen, G., Wever, D., Keijzer, E. *et al.* 2015. Injectivity Loss in Polymer Floods: Causes, Preventions and Mitigations. presented at the SPE Kuwait Oil and Gas Show and Conference, 2015/10/11/, Mishref, Kuwait.

Lee, K. 2012. *Impact of Fracture Creation and Growth on Well Injectivity and Reservoir Sweep During Waterflooding and Chemical Eor Processes.* Doctor of Philosophy, University of Texas at Austin.

Manichand, R.N.N., Moe Soe Let, K.P.P., Gil, L. *et al.* 2013. Effective Propagation of HPAM Solutions Through the Tambaredjo Reservoir During a Polymer Flood. *SPE Production & Operations*, **28**, 358-368, https://doi.org/10.2118/164121-PA.

Melo, M.A., Lins, A.G. and Silva, I.P.G. 2017. Lessons Learned From Polymer Flooding Pilots in Brazil. presented at the SPE Latin America and Caribbean Mature Fields Symposium, 2017/3/15/, Salvador, Bahia, Brazil.

Prats, M. 1961. Effect of Vertical Fractures on Reservoir Behavior-Incompressible Fluid Case. *Society of Petroleum Engineers Journal*, **1**, 105-118, https://doi.org/10.2118/1575-G.

Qi, P., Ehrenfried, D.H., Koh, H. *et al.* 2017. Reduction of Residual Oil Saturation in Sandstone Cores by Use of Viscoelastic Polymers. *SPE Journal*, **22**, 447-458, https://doi.org/10.2118/179689-PA.

Sagyndikov, M., Seright, R., Kudaibergenov, S. *et al.* 2022. Field Demonstration of the Impact of Fractures on Hydrolyzed Polyacrylamide Injectivity, Propagation, and Degradation. *SPE Journal*, **27**, 999-1016, https://doi.org/10.2118/208611-PA.

Seright, R.S. 1983. The Effects of Mechanical Degradation and Viscoelastic Behavior on Injectivity of Polyacrylamide Solutions. *Society of Petroleum Engineers Journal*, **23**, 475-485, https://doi.org/10.2118/9297-PA.

Seright, R.S. 2017. How Much Polymer Should Be Injected During a Polymer Flood? Review of Previous and Current Practices. *SPE Journal*, **22**, 1-18, https://doi.org/10.2118/179543-PA.

Seright, R.S., Seheult, J.M. and Talashek, T. 2009. Injectivity Characteristics of EOR Polymers. *SPE Reservoir Evaluation & Engineering*, **12**, 783-792, https://doi.org/10.2118/115142-PA.

Seright, R.S., Azad, M.S., Abdullah, M.B. *et al.* 2023. Effect of Residual Oil Saturation and Salinity on HPAM Rheology in Porous Media. *SPE Annual Technical Conference and Exhibition*.

Vela, S., Peaceman, D.W. and Sandvik, E.I. 1976. Evaluation of Polymer Flooding in a Layered Reservoir With Crossflow, Retention, and Degradation. *Society of Petroleum Engineers Journal*, **16**, 82-96, https://doi.org/10.2118/5102-pa.

Wang, D., Han, P., Shao, Z. *et al.* 2008. Sweep-Improvement Options for the Daqing Oil Field. *SPE Reservoir Evaluation & Engineering*, **11**, 18-26, https://doi.org/10.2118/99441-PA.

Zechner, M., Clemens, T., Suri, A. *et al.* 2015. Simulation of Polymer Injection Under Fracturing Conditions—An Injectivity Pilot in the Matzen Field, Austria. *SPE Reservoir Evaluation & Engineering*, **18**, 236-249, https://doi.org/10.2118/169043-PA.

Zechner, M., Buchgraber, M., Clemens, T. *et al.* 2013. Flow of Polyacrylamide Polymers in the Near-Wellbore-Region, Rheological Behavior within Induced Fractures and Near-Wellbore Area. presented at the SPE Annual Technical Conference and Exhibition.

Zeynalli, M., Al-Shalabi, E.W. and AlAmeri, W. 2022. An Extended Unified Viscoelastic Model for Predicting Polymer Apparent Viscosity at Different Shear Rates. *SPE Reservoir Evaluation & Engineering*, 1-23, https://doi.org/10.2118/206010-PA.